

Optical tomography complements light sheet microscopy for *in toto* imaging of zebrafish development

Andrea Bassi^{1,2}, Benjamin Schmid¹ and Jan Huisken^{1,*}

ABSTRACT

Fluorescently labeled structures can be spectrally isolated and imaged at high resolution in living embryos by light sheet microscopy. Multimodal imaging techniques are now needed to put these distinct structures back into the context of the surrounding tissue. We found that the bright-field contrast of unstained specimens in a selective plane illumination microscopy (SPIM) setup can be exploited for *in vivo* tomographic reconstructions of the three-dimensional anatomy of zebrafish, without causing phototoxicity. We report multimodal imaging of entire zebrafish embryos over several hours of development, as well as segmentation, tracking and automatic registration of individual organs.

KEY WORDS: SPIM, Fluorescence, Light sheet microscopy, Optical tomography, Time-lapse imaging, Zebrafish

INTRODUCTION

Our understanding of embryonic development relies fundamentally on the observation of morphogenesis in living organisms (Keller, 2013; Pantazis and Supatto, 2014). Fluorescence light sheet microscopy, such as selective plane illumination microscopy (SPIM; Huisken et al., 2004), has proven to be a powerful tool to image developmental processes *in vivo* with fast, high-resolution optical sectioning over large volumes (Huisken and Stainier, 2009). However, an intrinsic limitation of all fluorescence microscopy techniques, including SPIM, is their inability to image any structures beyond the labeled tissue. The fluorescent structures therefore appear out of context of the sample's anatomy and features such as the growth or migration of fluorescent tissue through the surrounding tissue may therefore be hard to interpret. The anatomy of fixed samples is commonly visualized by imaging autofluorescence, but this is not an option for *in vivo* studies because detection of the low-level, non-specific autofluorescence signal requires high illumination power, causing serious phototoxicity. It is therefore desirable to find a technique that delivers structural information of the unstained tissue to complement the fluorescence data.

Here we show that, without modifying any component of a typical SPIM setup, we can perform a multimodal acquisition that integrates the high-resolution SPIM fluorescence data with optical tomography, purely based on bright-field contrast. We present *in vivo* data of zebrafish to demonstrate that optical tomography is a valuable tool to observe the whole anatomy of living translucent organisms,

complementing and improving the analysis of SPIM data. We demonstrate that our multimodal system offers new possibilities to observe localised processes during zebrafish embryogenesis in a broader *in toto* context over several hours or days.

Optical projection tomography (OPT; Sharpe et al., 2002) had been developed to exploit the bright-field contrast of the sample by acquiring several light transmission images (or projections) from different directions; the 3D structure of the sample is then reconstructed using a back-projection algorithm (Kak and Slaney, 1988). Unfortunately, OPT and SPIM are incompatible, as OPT requires a long depth of field, ideally spanning the entire depth of the specimen, whereas SPIM benefits from a shallow depth of field. To overcome this incompatibility, hybrid OPT-SPIM instruments have recently been developed by reducing the numerical aperture (NA) of the detection unit to achieve the long depth of field needed for OPT (Arranz et al., 2013; Mayer et al., 2014). As a consequence, the overall resolution and contrast in the OPT reconstructions are compromised. Moreover, SPIM is considered an ideal technique to image development *in vivo*, whereas tomographic imaging is commonly believed suitable only for fixed and chemically cleared samples and, indeed, only a few *in vivo* applications have been reported (Colas and Sharpe, 2009; Bassi et al., 2011; McGinty et al., 2011). We decided to look for alternative solutions that would achieve tomographic reconstructions of living specimens in a high-resolution, high-NA SPIM setup without any modifications to the hardware.

RESULTS AND DISCUSSION

Implementation of optical tomography in a light sheet microscope

To integrate an optical tomography approach in a SPIM microscope we took advantage of three features of our existing SPIM setup: (1) fast image acquisition with high frame rate sCMOS cameras; (2) multiview capability, i.e. the sample can be quickly rotated; and (3) LED for back illumination, which can provide transmission images of the specimen. Owing to the relatively high NA of the detection lens (0.3), the depth of field δ_z is only $\sim 15 \mu\text{m}$ and does not span the depth of a typical sample in SPIM of $\sim 0.1\text{-}1 \text{ mm}$ (Fig. 1). Therefore, a stack of ~ 20 transmission images was taken by sliding the sample through the detection objective's plane of focus. The in-focus information was extracted by high-pass filtering the images and a weighted average yielded a projection of the sample with enhanced depth of field (Häusler, 1972) (supplementary material Methods). Since a projection represents an approximation of the line integral of light attenuation along a certain direction, by collecting multiple projections from several directions (typically 360) we created a dataset suitable for tomographic reconstruction; optically sectioned volumes of the samples were obtained by a filtered back-projection algorithm (Kikuchi and Sonobe, 1994; Fauver et al., 2005). No modification to the SPIM hardware or calibration was needed for the tomographic reconstruction. This

¹Max Planck Institute of Molecular Cell Biology and Genetics, Dresden 01307, Germany. ²Politecnico di Milano, Dipartimento di Fisica, Milano 20133, Italy.

*Author for correspondence (huisken@mpi-cbg.de)

This is an Open Access article distributed under the terms of the Creative Commons Attribution License (<http://creativecommons.org/licenses/by/3.0>), which permits unrestricted use, distribution and reproduction in any medium provided that the original work is properly attributed.

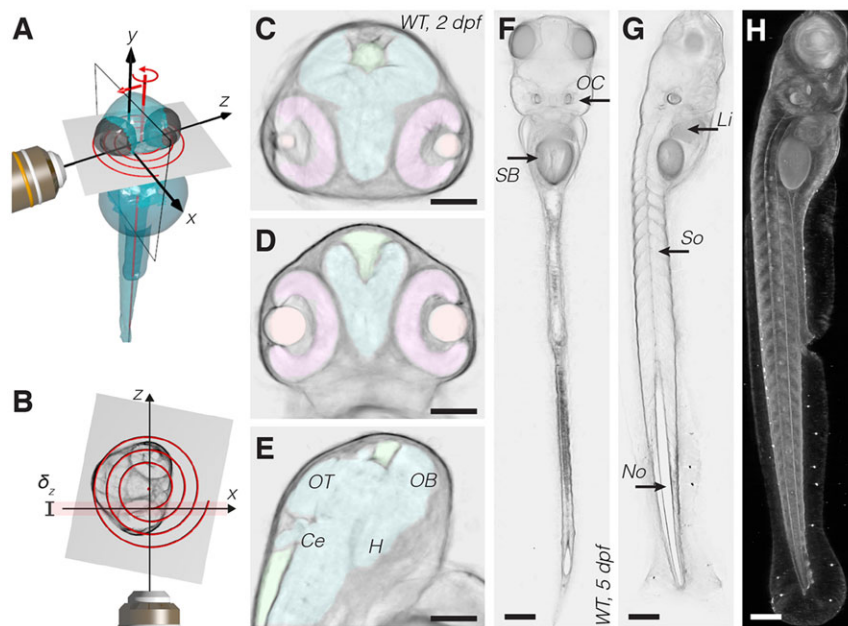


Fig. 1. Optical tomography principles and results.

(A) Scheme of the acquisition system. During the measurement the specimen is translated and rotated through the focal plane of the detection objective lens (x, y). The specimen is sampled along a spiral. (B) Scheme of the system from the top. The spiral is formed on the transverse section of the specimen. The detection objective's depth of field, δ_z , is highlighted in red. (C–E) Transverse (C), coronal (D) and sagittal (E) slices of a wild-type 2 dpf zebrafish head obtained *in vivo* with optical tomography (reconstructed virtual sections). Segmented head organs: retina (pink), eye lens (orange), brain ventricles (green), brain (cyan). Annotated brain domains: optic tectum (OT), hypothalamus (H), cerebellum (Ce) and olfactory bulb (OB). (F, G) Coronal (F) and sagittal (G) slices of a 5 dpf zebrafish. SB, swim bladder; OC, otic capsule; Li, liver; So, somites; No, notochord. (H) Lateral view of the 3D reconstructed sample. Scale bars: 100 μm .

method can therefore be readily adopted by a large number of systems, including commercial light sheet microscopes and simple SPIM implementations such as OpenSPIM (Pitrone et al., 2013; Gualda et al., 2013).

Tomographic acquisition is compatible with *in vivo* imaging

The acquisition of 360 image stacks for the tomographic reconstruction was initially performed sequentially, angle by angle, as commonly done for SPIM multiview acquisitions (Swoger et al., 2007). This process was not only time consuming, but also repeatedly exposed the sample to abrupt motion. In order to collect the tomography data more efficiently and avoid any detrimental effects on the sample, we developed a dedicated acquisition process: running the camera continuously at high frame rate, we turned the sample continuously and moved it smoothly through the detection image plane at the same time. Consequently, the image stacks necessary for the reconstruction were acquired in a spiral (Fig. 1A,B; supplementary material Movie 1). Typically, the spiral consisted of 20 complete rotations, images were acquired every 1° at 60 frames per second (fps), and the total acquisition of 7200 images took less than 2 min per specimen. We implemented a real-time processing routine to create projections with enhanced depth of field from the set of images belonging to each angle. Only the final 360 projections were saved to the hard drive for subsequent 3D reconstruction, reducing the amount of data by a factor of 20. The short acquisition times integrate well with the fast SPIM recording and make the measurement compatible with *in vivo* imaging and time-lapse observation of development.

Optical tomography delivers high-resolution 3D images of unstained zebrafish

To evaluate the quality of optical tomography we imaged living wild-type zebrafish at different stages of development, from 1 to 5 days post fertilization (dpf) and treated with PTU to remove pigmentation. The tomographic reconstruction has inherent isotropic resolution: the sample could be virtually sectioned and visualized along any desired direction (supplementary material Movie 2). Several regions in a 2 dpf zebrafish head were clearly defined by bright-field contrast in transverse, sagittal and coronal

sections (Fig. 1C–E). We applied semi-automatic segmentation (supplementary material Methods) based on gradient detection to highlight structures such as brain domains, brain ventricles and retinas (Mueller and Wullmann, 2005) (colored in Fig. 1C–E; supplementary material Fig. S1 and Movie 3). Organs of a known shape could be detected and segmented in an entirely automatic fashion; for example, the spherical eye lens was localized using a sphere recognition algorithm (Schmid et al., 2013). The resulting segmentations are in agreement with data obtained by confocal microscopy in fixed samples using nuclear staining (Ronneberger et al., 2012). Our technique also offered good penetration depth: we were able to reconstruct an entire 5 dpf zebrafish (Fig. 1F–H) by tiling four acquisitions at $10\times$ magnification. At larval stage (3–5 dpf), we identified and segmented internal organs, such as the liver, intestine, swim bladder and notochord (supplementary material Fig. S2). Hence, the tomographic reconstruction is useful on its own to observe zebrafish anatomy *in vivo* and to annotate, segment and quantitatively measure the volume of several organs.

The bright-field contrast complements the fluorescence signal

To assess the value of the multimodal imaging, we recorded and superimposed optical tomography and SPIM volumes of a *Tg(neurog1:GFP)×Tg(kdrl:rasCherry)* embryo expressing green fluorescent protein (GFP) in neuronal cells and mCherry in endothelial cells. The fluorescence detected with SPIM was sparse and difficult to assign to any anatomical region (Fig. 2A,C). Only the additional optical tomography information placed the fluorescence data in the proper anatomical context within the zebrafish in all of the reconstructed sections (Fig. 2B,D; supplementary material Fig. S3) and in the entire volume (Fig. 2E,F; supplementary material Movie 4). Registration of the two modalities was straightforward, as both datasets were acquired using the same detector in short succession (supplementary material Fig. S4). Only the relative z -position of the reconstructed volume had to be determined by registration (supplementary material Fig. S5). We conclude that the multimodal system provides a comprehensive visualization of the specimen, making it well suited

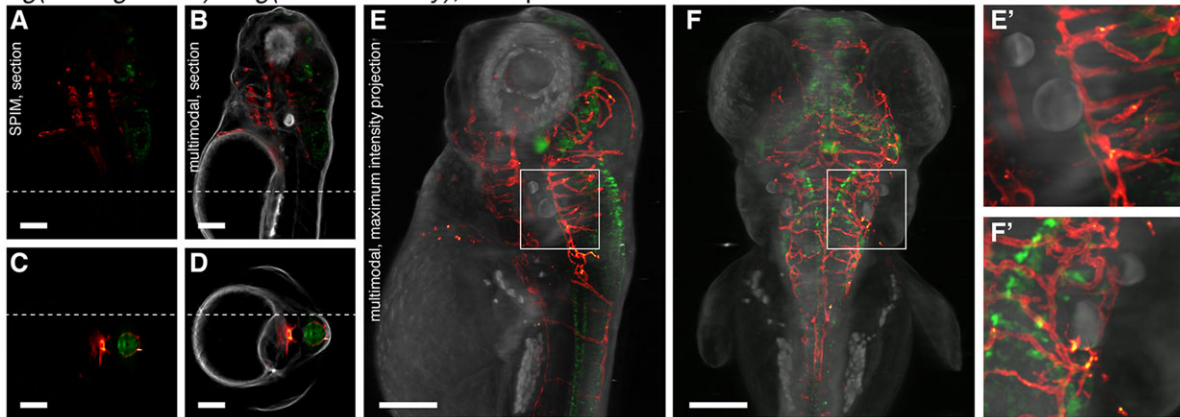
Tg(neurog1:GFP) x Tg(kdrl:rasCherry), 3.5 dpf

Fig. 2. Multimodal imaging. (A-D) Sagittal (A,B) or transverse (C,D) slice of a transgenic *Tg(neurog1:GFP)×Tg(kdrl:rasCherry)* zebrafish (3.5 dpf) visualized with (A,C) SPIM or (B,D) SPIM (red/green) combined with optical tomography (gray). The dotted lines in the sagittal sections indicate the position of the transverse section and vice versa. (E-F') Lateral (E) and dorsal (F) views of the sample created with weighted intensity projection. The boxed regions in E,F are enlarged in E',F' to illustrate the fine details in the data. Scale bars: 100 μ m.

for *in vivo* localization analysis of gene expression in the entire zebrafish.

Multimodal acquisition of organogenesis in zebrafish

In order to demonstrate the value of the system for the analysis of embryogenesis, we captured the course of development of a *Tg(kdrl:GFP)* zebrafish from the early embryo to the larval stage at 10 min intervals with both modalities in parallel (Fig. 3; supplementary material Movie 5). The development of the fluorescent vasculature was acquired at single-cell resolution with SPIM, while the tomographic reconstruction was used to visualize not only the outline of the sample but also the entire volume of the zebrafish anatomy to analyze single organ development. An example is shown in supplementary material Fig. S6, where we visualized head development from 36 to 60 h post fertilization (hpf). Since the head undergoes drastic modifications in a few hours of growth, we registered the time-lapse reconstructions onto a reference system based on the fish anatomy; the positions of the eyes were automatically detected at each time point (supplementary material Methods) and used as landmarks (supplementary material Fig. S6 and Movie 6). This procedure allowed us to observe any location of the head during the entire time-lapse together with the formation of cranial vasculature, such as the development of the primordial hindbrain channels over a single section. We conclude

that the multimodal acquisition offers the possibility to localize, track and register specific anatomical regions of the sample, facilities that are not readily available using fluorescence modalities.

Conclusions

We have demonstrated how optical tomography complements light sheet microscopy, providing a 3D reconstruction with label-free bright-field contrast. The additional information is quickly acquired in between the regular SPIM recordings and is practically free of phototoxicity. We introduced an efficient routine based on a spiral acquisition to extend the depth of field of the microscope without sacrificing image resolution and contrast. Only the relevant data were saved for the tomographic reconstruction. The described multimodal acquisition offers a complete picture of the developing sample, which is particularly valuable when the expression of fluorescence reporters is sparse and scattered across different anatomical regions. The ability to create a reference system based on the anatomy of the sample is not only very valuable for time-lapse registration, but also is essential for the analysis of multiple samples: being able to see the outline of the sample, track internal organs and orient the reconstructed data to a common reference system is indispensable in order to compare multiple samples and perform statistical analysis. Abnormal development and morphological defects (such as edemas, damaged yolk), which may be undetectable using fluorescence imaging, are

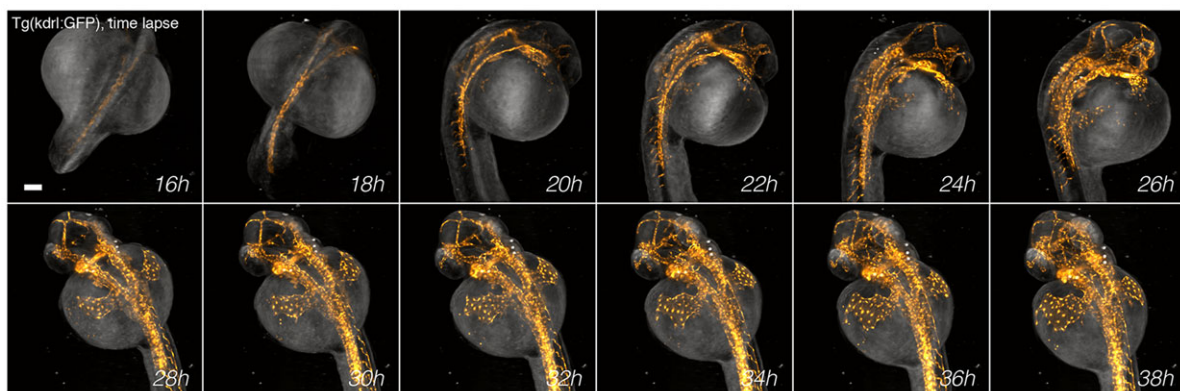


Fig. 3. Long-term time-lapse. Time-lapse development of a *Tg(kdrl:GFP)* zebrafish from 16-38 hpf acquired every 10 min. SPIM signal (yellow) is superimposed on tomographic reconstruction (gray). The optical tomography data are inverted in all panels. Scale bar: 100 μ m.

easily detected in transmission and their extent can be quantified during development. Since no staining of the sample is required, the technique is highly suited to the study of emerging model organisms, in which genetic tools and fluorescent transgenic lines are yet to be established.

MATERIALS AND METHODS

Fish lines and sample preparation

Zebrafish (*Danio rerio*) adults and embryos were kept at 28.5°C and were handled according to established protocols (Nüsslein-Volhard and Dahm, 2002) and in accordance with EU directive 2011/63/EU as well as the German Animal Welfare Act. Wild-type zebrafish (AB and TL strains) were used for tomographic imaging. The fluorescent transgenic lines *Tg(kdrl:rasCherry)* (Chi et al., 2008), *Tg(kdrl:GFP)* (Jin et al., 2005) and *Tg(fli:GFP)* (Lawson and Weinstein, 2002) were used to image the vasculature with SPIM and *Tg(neurog1:GFP)* (Andersen et al., 2011) to visualize the nervous system. At 24 hpf the embryos were treated with 0.2 mM 1-phenyl 2-thiourea (PTU; Sigma) to inhibit pigmentation. During imaging, the samples were anesthetized with 200 mg/l Tricaine (Sigma) and embedded in low melting point agarose (Sigma) as described previously (Kaufmann et al., 2012): for single time point acquisition, the samples were embedded in 1.5% agarose inside glass capillaries, for long-term time-lapse acquisition the samples were embedded in 0.1% agarose inside fluorinated ethylene propylene (FEP) tubes (S1815-04, Bolla). The imaging chamber was filled with E3 medium (Nüsslein-Volhard and Dahm, 2002) containing 200 mg/l Tricaine.

Setup

We used the SPIM setup previously described by Schmid et al. (2013) (supplementary material Fig. S4). The four-lens SPIM system consisted of four identical water-dipping objectives (UMPLFLN 10×/0.3, Olympus). One of the four objectives was used for detection. Two objectives, perpendicular to the detection objective, were used for double-sided SPIM illumination. The fourth objective was used for transmission illumination. A red LED backlight (MDBL-CR25, MLEK-A080W1LR, Moritex Schott) was placed behind this objective, providing illumination at high NA. For SPIM illumination, a multicolor laser light engine (SOLE-6, Omicron) with a 488 nm (200 mW) and a 561 nm (150 mW) laser was used. The laser beam was split 50/50 and directed through a chopper wheel (MC1F10, Thorlabs) to illuminate the sample consecutively from opposing directions. Each beam was sent onto a resonant galvanometric mirror (1 kHz, EOPC), which pivots the light sheet and reduces shadowing effects in the excitation paths due to absorption in the specimen (Huisken and Stainier, 2007). Light sheets were generated with cylindrical lenses ($f=50$ mm) and projected with telescopes and the illumination objectives onto the focal plane of the detection lens. The focal plane of the detection objective was imaged onto an sCMOS camera (Zyla, Andor). The camera captured images of a field of view of ~ 1 mm² at 30–100 fps. A filter wheel (96A354, LUDL Electronics) was used to select the transmission/fluorescence signal at the desired wavelength ranges. The sample was dipped into the medium-filled imaging chamber from the top and was translated along the z -axis with a linear stage (M-404.1PD, Physik Instrumente) and rotated with a rotational stage (M-660.55, Physik Instrumente). Although not strictly necessary, it was convenient to position the sample close to the rotation axis before the acquisition (Cheddad et al., 2012). To this end, we designed a sample holder that incorporated a dual axis translation mount (LM1XY, Thorlabs) and allowed the user to manually move the sample in two directions and center it on the rotation axis (supplementary material Fig. S7).

Spiral acquisition

A LabVIEW (National Instruments) program was implemented to adjust the stage positions, filter wheels and illumination power. During the spiral acquisition of the tomographic dataset the sample was continuously rotated while the translation stage moved the sample along the optical axis of the detection objective (z -axis). Typically, 20 complete rotations were performed

while the sample was translated over a distance of ~ 500 μ m. The speed of the translation motor (typically 4 μ m/s) and the rotation stage (typically 60°/s) were adjusted according to the desired frame rate (typically 60 Hz). The motors moved continuously from the initial to the final positions while the camera was acquiring the images. To ensure precise synchronization throughout the acquisition, the controller of the motor and the camera received a common digital trigger at the beginning of the acquisition. Typically, 7200 images corresponding to 20 different positions from 360 angles were acquired. The exposure time was typically 16 ms using the rolling shutter mode of the sCMOS camera or shorter (2 ms) using the global shutter mode. We did not observe any differences in the results obtained with the two shuttering modalities. The acquisition of the entire dataset required ~ 2 min for tomography. The LED was on during the entire spiral acquisition and its power was manually adjusted before the acquisition to use the full dynamic range of the camera. Acquisition settings, such as frame rate, exposure time and gain, were controlled with a Fiji plugin (Schindelin et al., 2012), which used the Java Native Interface for function calls into the Andor Software Development Kit. The same Fiji plugin was used to read the images from the camera, for real-time processing and to generate and save the projections with enhanced depth of field. For details of depth of field enhancement, see supplementary material Methods and Fig. S8.

Tomographic reconstruction

The position of the rotational axis in the x,y -plane was determined as described by Walls et al. (2005) before tomographic reconstruction. Briefly, a series of images was reconstructed with differently assumed x -positions of the rotational axis, and the variance of each image was calculated. The reconstructed image with the maximum variance is the least blurred and is closest to the ideal reconstruction. The corresponding position of the rotational axis was assumed to be the correct one.

Reconstructions were performed in MATLAB (MathWorks) using a back-projection algorithm based on inverse Radon transform (Kak and Slaney, 1988). Transverse sections of the sample were created for each y -position of the field of view and the reconstruction was repeated slice by slice to create the 3D volumes (supplementary material Movie 2). The reconstruction required 0.1 to 1 s per transverse section (depending on the region of interest) using a single processor of a Xeon CPU (Intel). In order to reduce possible artifacts resulting from non-uniform illumination and the noise of the camera we implemented a background division and a dark noise subtraction routine (Walls et al., 2005) in the acquisition plugin.

For further details of segmentation and visualization, see supplementary material Methods.

SPIM acquisition

The acquisition of the SPIM stacks was performed at the end of the spiral acquisition. The LED was turned off, the filter wheel on the detection arm was switched to the position corresponding to the desired fluorescence channel and the sample was oriented to the desired angle using the rotational stage. The speed of the translation motor was chosen such that, for the given frame rate (60 Hz), a z -spacing between consecutive frames of typically 2 μ m was achieved. The sample was moved along the z -direction continuously from the initial to the final position while the camera was acquiring the images and the laser was triggered only during each exposure. Typically, 300 frames were acquired in 5 s. One or more fluorescence channels were acquired sequentially and the sample was then rotated to the next detection angle. Typically, four angles were acquired.

Alignment of SPIM with optical tomography

The back-projection algorithm reconstructed 3D volumes composed of transverse sections centered on the rotational axis of the system. In order to overlap this reconstruction with the SPIM volume, we determined the position of the SPIM stack relative to the rotation axis. Since the two imaging modalities used the same detector, the datasets were inherently aligned along the x - and y -directions. We determined the z -position of the rotational axis using the SPIM data, acquiring stacks of the fluorescent sample from two different views (e.g. $\theta=0^\circ$ and $\theta=90^\circ$): one stack was used as a reference, while the second stack was reshaped and registered to the first

stack using a 1D translation (supplementary material Fig. S5). The process was performed once per imaging session.

Acknowledgements

We thank I. Büttner for help with sample preparation, D. Kainmüller for help with segmentation analysis and J. Swoger for discussions on data analysis.

Competing interests

The authors have filed a patent that relates to some aspects of this work.

Author contributions

A.B. and J.H. conceived and designed the experiments. A.B. and B.S. performed the experiments and analyzed the data. All authors wrote the manuscript.

Funding

This research was funded by the People Programme (Marie Curie Actions) of the European Union's Seventh Framework Programme [FP7/2007-2013] under REA grant agreement no. PIEF-GA-2012-330186 (to A.B.) and generous funding by the Max Planck Society (to J.H.). Deposited in PMC for immediate release.

Supplementary material

Supplementary material available online at <http://dev.biologists.org/lookup/suppl/doi:10.1242/dev.116970/-/DC1>

References

- Andersen, E. F., Asuri, N. S. and Halloran, M. C. (2011). In vivo imaging of cell behaviors and F-actin reveals LIM-HD transcription factor regulation of peripheral versus central sensory axon development. *Neural Dev.* **6**, 27.
- Arranz, A., Dong, D., Zhu, S., Rudin, M., Tsatsanis, C., Tian, J. and Ripoll, J. (2013). Helical optical projection tomography. *Opt. Express* **21**, 25912-25925.
- Bassi, A., Fieramonti, L., D'Andrea, C., Mione, M. and Valentini, G. (2011). In vivo label-free three-dimensional imaging of zebrafish vasculature with optical projection tomography. *J. Biomed. Opt.* **16**, 100502.
- Cheddad, A., Svensson, C., Sharpe, J., Georgsson, F. and Ahlgren, U. (2012). Image processing assisted algorithms for optical projection tomography. *IEEE Trans. Med. Imaging* **31**, 1-15.
- Chi, N. C., Shaw, R. M., De Val, S., Kang, G., Jan, L. Y., Black, B. L. and Stainier, D. Y. R. (2008). Foxn4 directly regulates tbx2b expression and atrioventricular canal formation. *Genes Dev.* **22**, 734-739.
- Colas, J.-F. and Sharpe, J. (2009). Live optical projection tomography. *Organogenesis* **5**, 211-216.
- Fauver, M., Seibel, E., Richard Rahn, J., Meyer, M. G., Patten, F. W., Neumann, T. and Nelson, A. C. (2005). Three-dimensional imaging of single isolated cell nuclei using optical projection tomography. *Opt. Express* **13**, 4210-4223.
- Gualda, E. J., Vale, T., Almada, P., Feijó, J. A., Martins, G. G. and Moreno, N. (2013). OpenSpinMicroscopy: an open-source integrated microscopy platform. *Nat. Methods* **10**, 599-600.
- Häusler, G. (1972). A method to increase the depth of focus by two-step image processing. *Opt. Commun.* **6**, 38-42.
- Huisken, J. and Stainier, D. Y. R. (2007). Even fluorescence excitation by multidirectional selective plane illumination microscopy (mSPIM). *Opt. Letters* **32**, 2608-2610.
- Huisken, J. and Stainier, D. Y. (2009). Selective plane illumination microscopy techniques in developmental biology. *Development* **136**, 1963-1975.
- Huisken, J., Swoger, J., Del Bene, F., Wittbrodt, J. and Stelzer, E. H. K. (2004). Optical sectioning deep inside live embryos by selective plane illumination microscopy. *Science* **305**, 1007-1009.
- Jin, S.-W., Beis, D., Mitchell, T., Chen, J.-N. and Stainier, D. Y. R. (2005). Cellular and molecular analyses of vascular tube and lumen formation in zebrafish. *Development* **132**, 5199-5209.
- Kak, A. C. and Slaney, M. (1988). *Principles of Computerized Tomographic Imaging*. IEEE Press.
- Kaufmann, A., Mickoleit, M., Weber, M. and Huisken, J. (2012). Multilayer mounting enables long-term imaging of zebrafish development in a light sheet microscope. *Development* **139**, 3242-3247.
- Keller, P. J. (2013). Imaging morphogenesis: technological advances and biological insights. *Science* **340**, 1234-1268.
- Kikuchi, S. and Sonobe, K. (1994). Three-dimensional computed tomography for optical microscopes. *Opt. Commun.* **107**, 432-444.
- Lawson, N. D. and Weinstein, B. M. (2002). In vivo imaging of embryonic vascular development using transgenic zebrafish. *Dev. Biol.* **248**, 307-318.
- Mayer, J., Robert-Moreno, A., Danuser, R., Stein, J. V., Sharpe, J. and Swoger, J. (2014). OPTISPIIM: integrating optical projection tomography in light sheet microscopy extends specimen characterization to non-fluorescent contrasts. *Opt. Lett.* **39**, 1053-1056.
- McGinty, J., Taylor, H. B., Chen, L., Bugeon, L., Lamb, J. R., Dallman M. J. and French, P. M. W. (2011). In vivo fluorescence lifetime optical projection tomography. *Biomed. Opt. Express* **2**, 1340-1350.
- Mueller, T. and Wullimann, M. F. (2005). *Atlas of Early Zebrafish Brain Development: A Tool for Molecular Neurogenetics*. Elsevier.
- Nüsslein-Volhard, C. and Dahm, R. (2002). *Zebrafish: A Practical Approach*, 1st edn. Oxford University Press.
- Pantazis, P. and Supatto, W. (2014). Advances in whole-embryo imaging: a quantitative transition is underway. *Nat. Rev. Mol. Cell Biol.* **15**, 327-339.
- Pitrone, P. G., Schindelin, J., Stuyvenberg, L., Preibisch, S., Weber, M., Eliceiri, K. W., Huisken, J. and Tomancak, P. (2013). OpenSPIM: an open access light sheet microscopy platform. *Nat. Methods* **10**, 598-599.
- Ronneberger, O., Liu, K., Rath, M., Rueß, M., Mueller, T., Skibbe, H., Drayer, B., Schmidt, T., Filippi, A., Nitschke, R. et al. (2012). ViBE-Z: a framework for 3D virtual colocalization analysis in zebrafish larval brains. *Nat. Methods* **9**, 735-742.
- Schindelin, J., Arganda-Carreras, I., Frise, E., Kaynig, V., Longair, M., Pietzsch, T., Preibisch, S., Rueden, C., Saalfeld, S., Schmid, B., et al. (2012). Fiji: an open-source platform for biological-image analysis. *Nat. Methods* **9**, 676-682.
- Schmid, B., Shah, G., Scherf, N., Weber, M., Thierbach, K., Campos, C. P., Roeder, I., Aanstad, P. and Huisken, J. (2013). High-speed panoramic light-sheet microscopy reveals global endodermal cell dynamics. *Nat. Commun.* **4**, 2207.
- Sharpe, J., Ahlgren, U., Perry, P., Hill, B., Ross, A., Hecksher-Sørensen, J., Baldock, R. and Davidson, D. (2002). Optical projection tomography as a tool for 3D microscopy and gene expression studies. *Science* **296**, 541-545.
- Swoger, J., Verveer, P., Greger, K., Huisken, J. and Stelzer, E. H. K. (2007). Multi-view image fusion improves resolution in three-dimensional microscopy. *Opt. Express* **15**, 8029-8042.
- Walls, J. R., Sled, J. G., Sharpe, J. and Henkelman, R. M. (2005). Correction of artefacts in optical projection tomography. *Phys. Med. Biol.* **50**, 4645-4665.

Supplementary Methods | Depth of field enhancement, segmentation and visualization.

Depth of field enhancement. Depth of field (DOF) enhancement was achieved by merging a stack of images collected at different z -positions into a single entirely focused projection (Fauver et al., 2005). To create the projection, one could simply sum the stack of images but this would create a blurred projection and consequently a blurred reconstruction, not optimal to visualize the details of the anatomy (**supplementary material Fig. S8**). We therefore employed an algorithm that relies on a high-pass criterion, which was applied to each image in the stack to extract in-focus regions. Given N images I_i , acquired at different z -positions, the projection with extended depth of field, I^E , was created as:

$$I^E = \frac{\sum_{i=1}^N I_i \cdot |I_i^{HP}|}{\sum_{i=1}^N |I_i^{HP}|}$$

where I_i^{HP} is a high pass replica of the acquired image. We used a fast method to generate the high pass images I_i^{HP} , in order to be compatible with real-time processing: we calculated the resulting value from the subtraction of the image I_i with its low pass replica, which was created by applying a moving average filter (with a kernel radius of ca. 10 μm) to I_i .

We tested an alternative way to extend the depth of field, which consisted in the acquisition of a stack of images, deconvolution of the images using the microscope's point spread function, and summing the deconvolved images to create the projection. The deconvolution was performed in Matlab (MathWorks) using a Richardson–Lucy algorithm. The method requires intense computation (not being compatible with real time processing) but has the advantage to quantitatively reconstruct the light attenuation coefficient within the sample. We used the results obtained with deconvolution as a landmark, to assess the quality of the results given by the high pass filter criterion. Visual comparison between the two methods shows good agreement (**supplementary material Fig. S8**).

Segmentation of organs and tracking of the eyes lenses. We developed a Fiji (Schindelin et al., 2012) algorithm to detect the zebrafish eye lenses, taking advantage of their spherical shape. We locally fitted a sphere to each lens using an intensity-based approach. Local search was used to adjust the parameters of a sphere (3D position and radius) to minimize the mutual information between the image data and an artificial sphere, which was constructed by drawing a sphere surface of 5 pixels width onto a black background. For the calculation of the mutual information only pixels inside the sphere were used.

During time-lapse experiments, we registered the reconstructed head volumes using the eye positions as landmarks: the position of the eye lenses was automatically detected in all the reconstructed volumes. From the coordinates of both lenses a rotational matrix was calculated and applied to align the eyes horizontally in the x,y -reference system. The fluorescence volume obtained with SPIM was aligned accordingly, applying the same

rigid transformation. Initial guesses for the eye positions of the first time point were provided manually, for each subsequent time point the results of the previous time point were used for initialization.

Organs and subdomain segmentation. Organ segmentation was performed using the segmentation tools of Amira software (FEI Visualization Sciences Group, USA). The borders of the region were highlighted in sections of the three-dimensional reconstructed volume. This was performed using a feature of the software that forces the highlighted border to lie on an automatically detected edge. The borders were manually highlighted in three to five sections, along three perpendicular directions. The software then allowed the user to automatically create a three-dimensional segmentation volume that included the highlighted borders and interpolated the volume using a gradient-based detection.

Visualization. Sections and 3D volumes were visualized using Fiji (Schindelin et al., 2012). In order to generate weighted intensity projections (**Fig. 2** and **supplementary materials Fig. S3**) of a 3D data stack, each image of the stack was first multiplied by a weighting factor. The factor varied linearly from 1 (first slice) to 0.5 (last slice). Then, a maximum intensity projection was performed. Compared to simple maximum intensity projection this method provided more details on one side of the sample and was useful to visualize the obtained results from different angles.

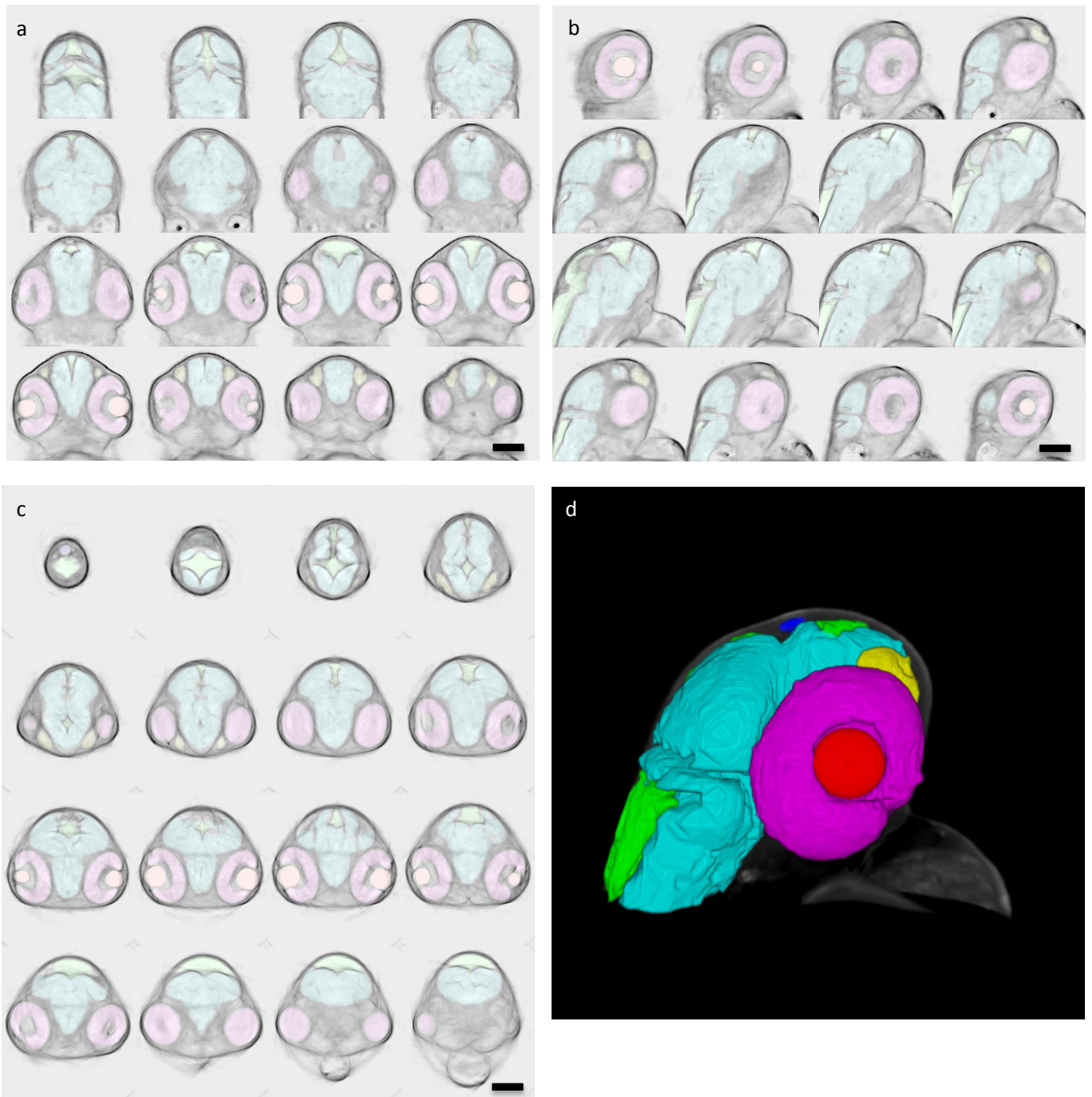


Figure S1 | Sections of a zebrafish head at 2dpf

(a) Coronal, (b) sagittal and (c) transverse slices of a 2 dpf zebrafish head reconstructed with optical tomography. The superimposed colors indicate segmented head organs: retina (pink), eye lens (orange), brain ventricles (green), brain (cyan), olfactory pit (yellow), epiphysis (blue). (d) Three-dimensional reconstruction of the head showing the segmented organs. Slices are spaced 20 μm . Scale bar is 100 μm .

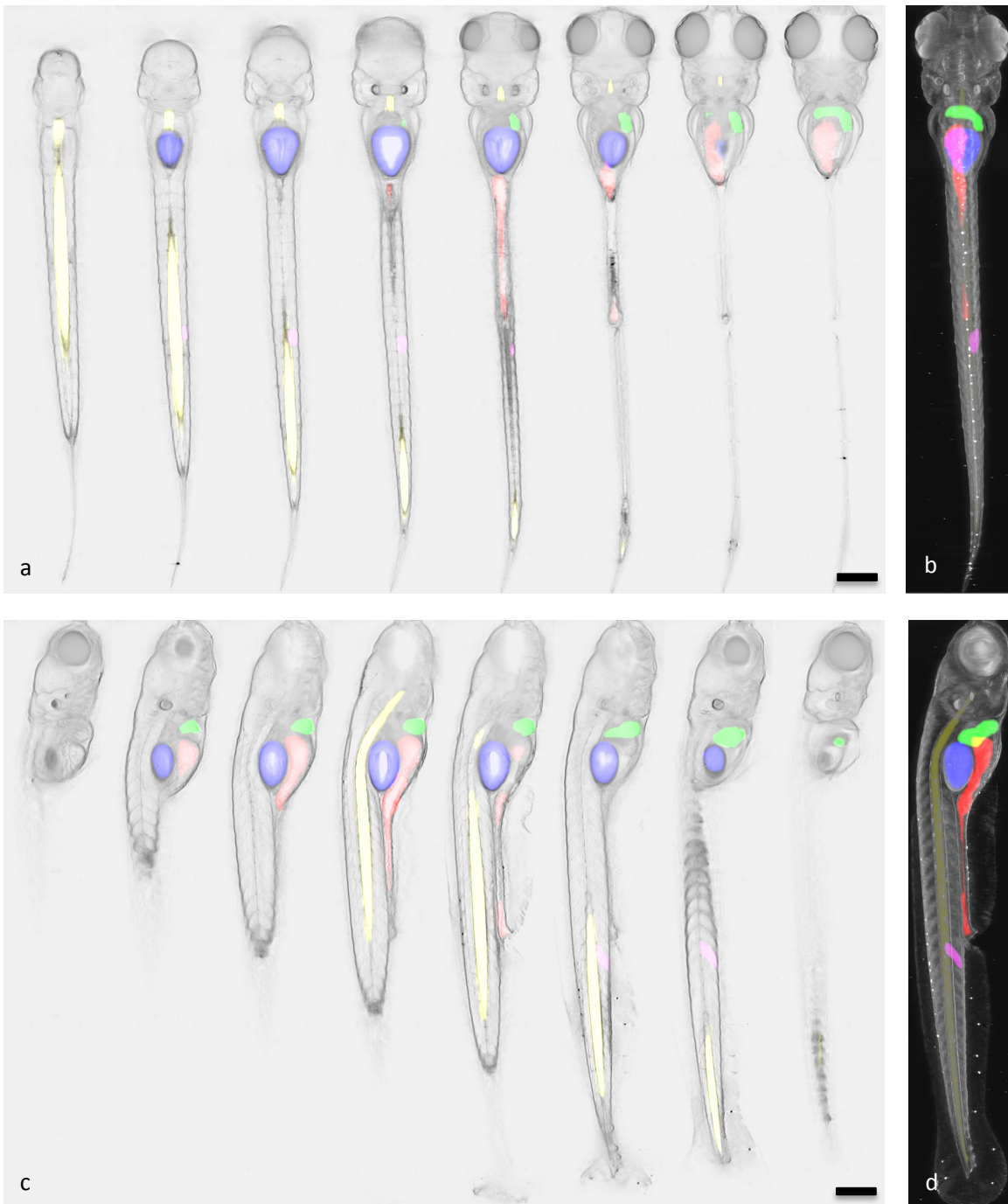


Figure S2 | Sections of an entire zebrafish at 5 dpf

(a) Coronal sections of an entire 5 dpf zebrafish reconstructed with optical tomography. The superimposed colors indicate segmented organs: liver (green), swim bladder (blue), gut (red), notochord (yellow), one single somite (pink). **(b)** Dorsal view of the 3D reconstructed sample. **(c)** Sagittal sections and **(d)** lateral view of the 3D reconstructed sample. Slices are spaced 45 μm . Scale bar is 200 μm .

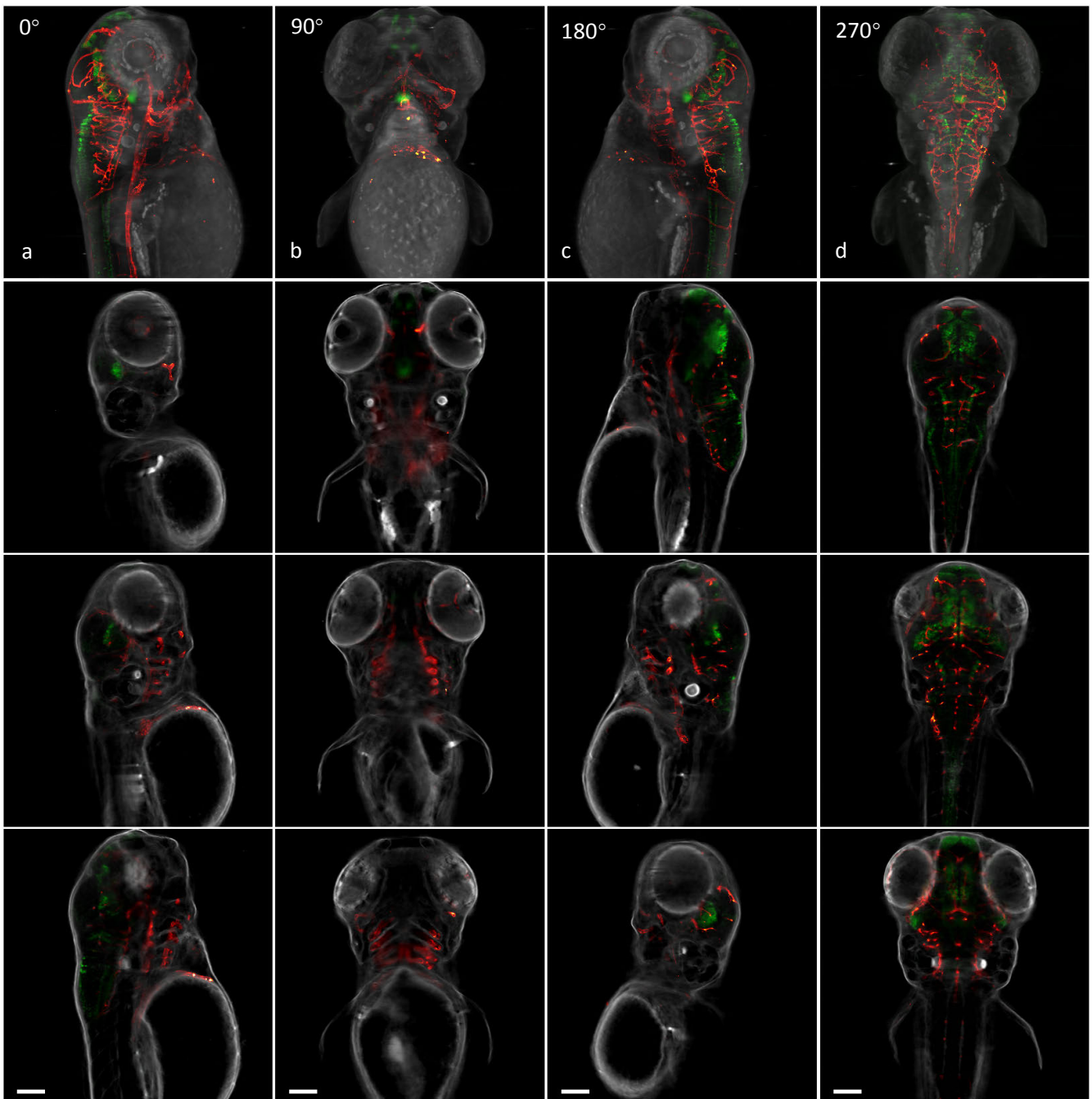


Figure S3 | Multimodal sections

Transgenic *Tg(neurogl1:GFP)* x *Tg(kdrl:rasCherry)* zebrafish (3.5 dpf) visualized at different orientations. SPIM (red/green) is superimposed with the inverted optical tomography contrast (gray). **(a)** Lateral view created by weighted maximum intensity projection (first row) and single sections (rest) from the left side to the center of the sample. **(b)** Frontal view, and single sections from the center to the front of the sample. **(c)** Lateral view, and single sections from the center to the right side of the sample. **(d)** Dorsal view, and single sections from the back to the center of the sample. Slices are spaced 65 μm . Scale bar is 100 μm .

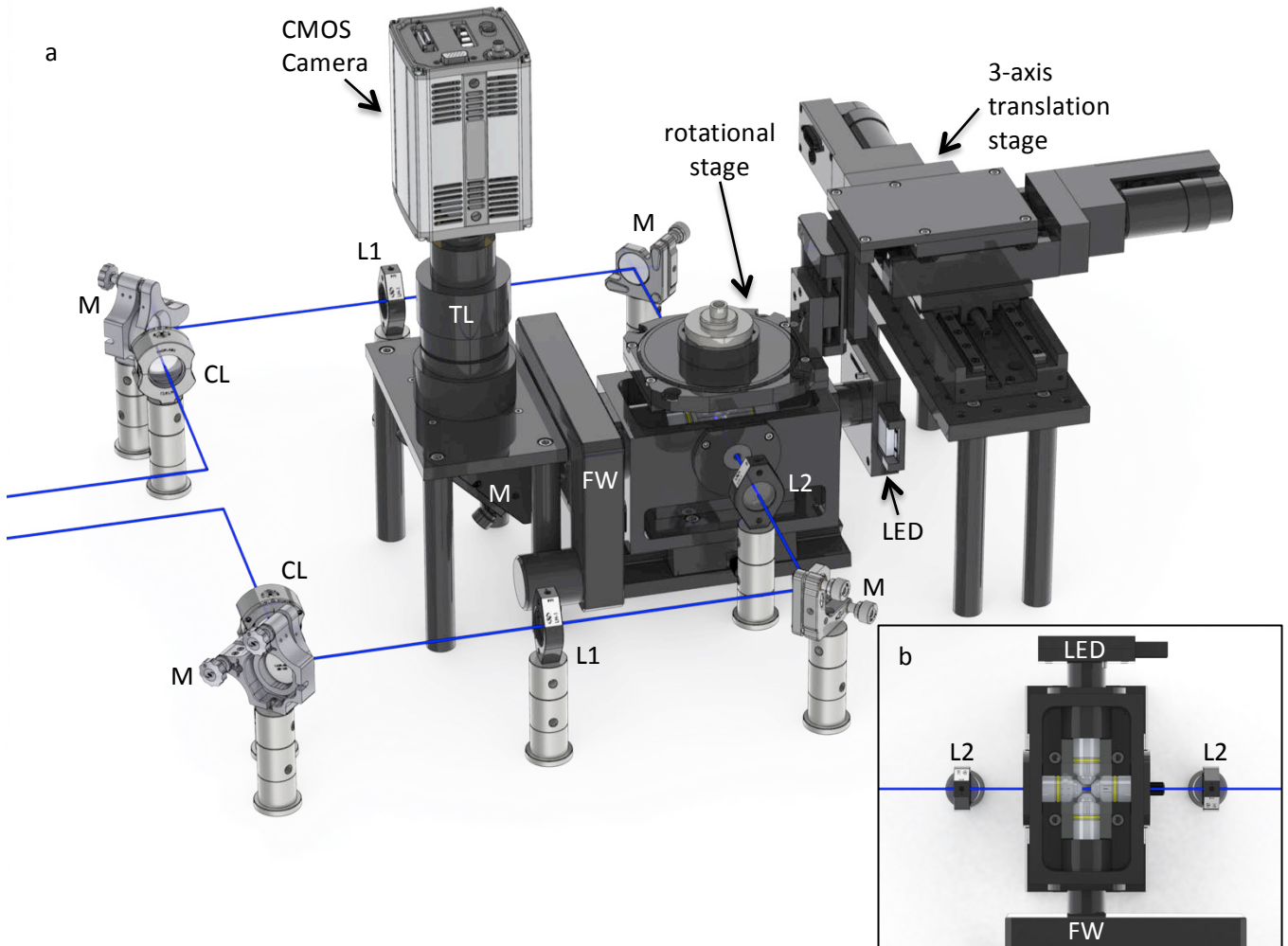


Figure S4 | Optical setup

(a) Schematic of the microscope setup. Each laser beam used for bidirectional SPIM illumination (blue) is passed through a cylindrical lens (CL), a telescope (lenses L1 and L2) and sent to the imaging chamber through an illumination lens. Two 45° mirrors (M) are used to properly align each beam. Brightfield illumination is provided in transmission mode by an LED backlight. The sample dips into the medium-filled imaging chamber from the top. It is held and moved by a fast rotational stage and a 3-axis linear stage. The image of the sample is formed at the detector using a water-dipping objective and a tube lens (TL). The detected light is passed through a filter wheel (FW) and a 45° mirror (M). **(b)** Top view of the imaging chamber. Illumination and detection are provided by four water-dipping objectives. Light-sheets illuminate the sample from two opposite sides (blue beams) and brightfield illumination is provided by an LED backlight, placed at the back of one of the objective. The transmitted or fluorescence light is collected by a fourth objective and passed through the filter wheel (FW).

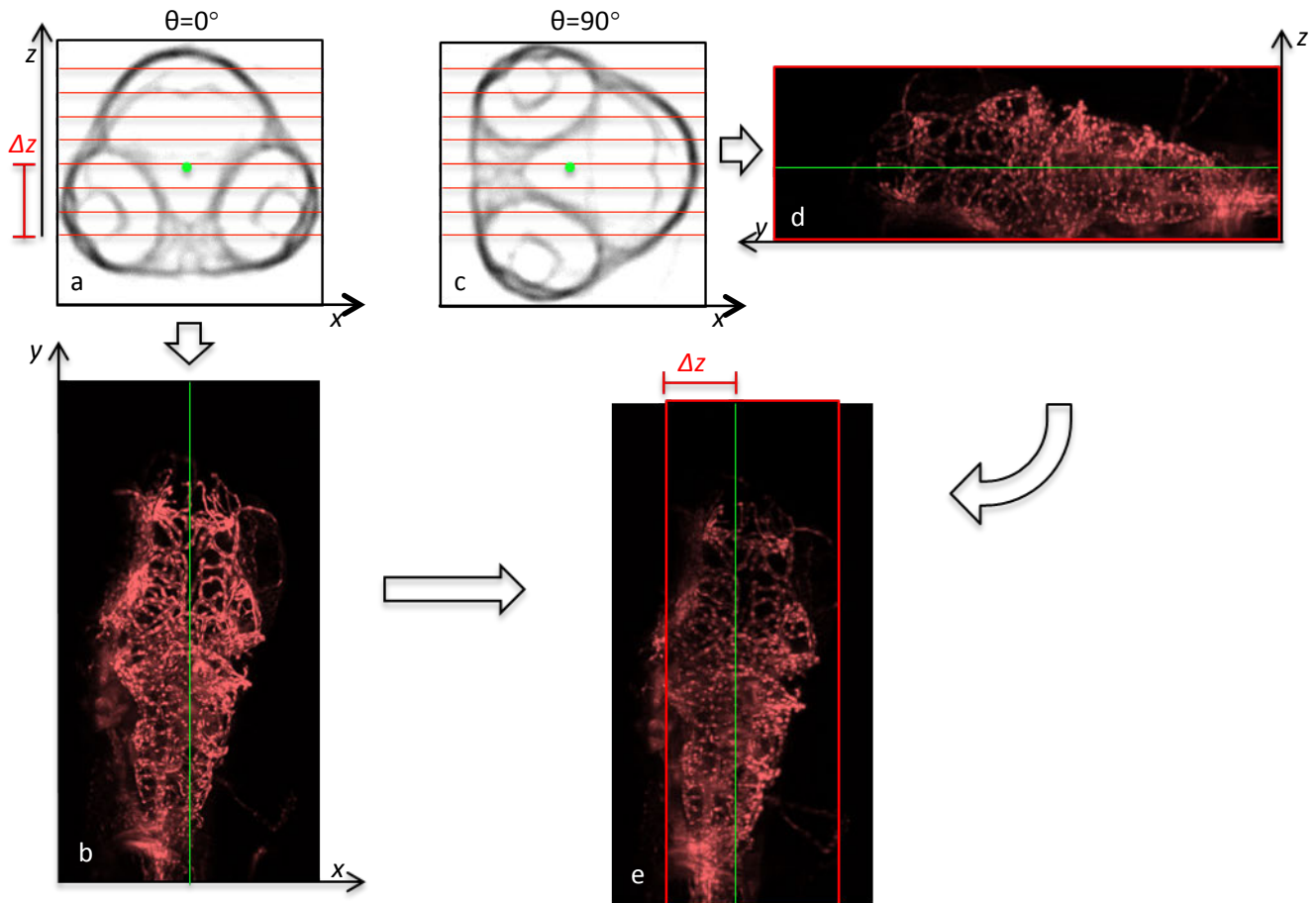


Figure S5 | Alignment of SPIM with optical tomography

(a) Transverse section of the sample oriented at a certain angle $\theta=0^\circ$. Optical tomography based on inverse Radon transform reconstructs squared sections centered on the axis of rotation of the system (green dot). Single planes acquired with SPIM are indicated as red lines in the images. The distance Δz (between the first image of the SPIM stack and the axis of rotation) is initially unknown (b) Projection along z of the SPIM stack acquired with the sample oriented at $\theta=0^\circ$. (c) Transverse section of the sample rotated at $\theta=90^\circ$. (d) Projection along x of the SPIM stack acquired with the sample oriented at $\theta=90^\circ$. (e) The distance Δz is determined by registering image (d) to image (b), according to the following procedure:

- 1) Acquire a stack of SPIM images with the sample oriented at angle $\theta=0^\circ$.
- 2) Sum these SPIM images to create a projection along the direction z , as shown in image (b).
- 3) Rotate the sample to $\theta=90^\circ$ and acquire another stack of SPIM images.
- 4) Reshape this SPIM stack (acquired at point 3) and create a projection along the direction x , as shown in image (d).
- 5) Image (b) and image (d) show the sample from the same view. Register these two images translating them horizontally as shown in image (e). The distance between the left side of image (e) and the center of image (d) is the distance Δz . This distance indicates the location of the SPIM stack relative to the center of rotation of the sample (green line).
- 6) Repeat the procedure at four different initial angles in order to determine Δz with pixel resolution. Use more angles to achieve sub-pixel resolution.

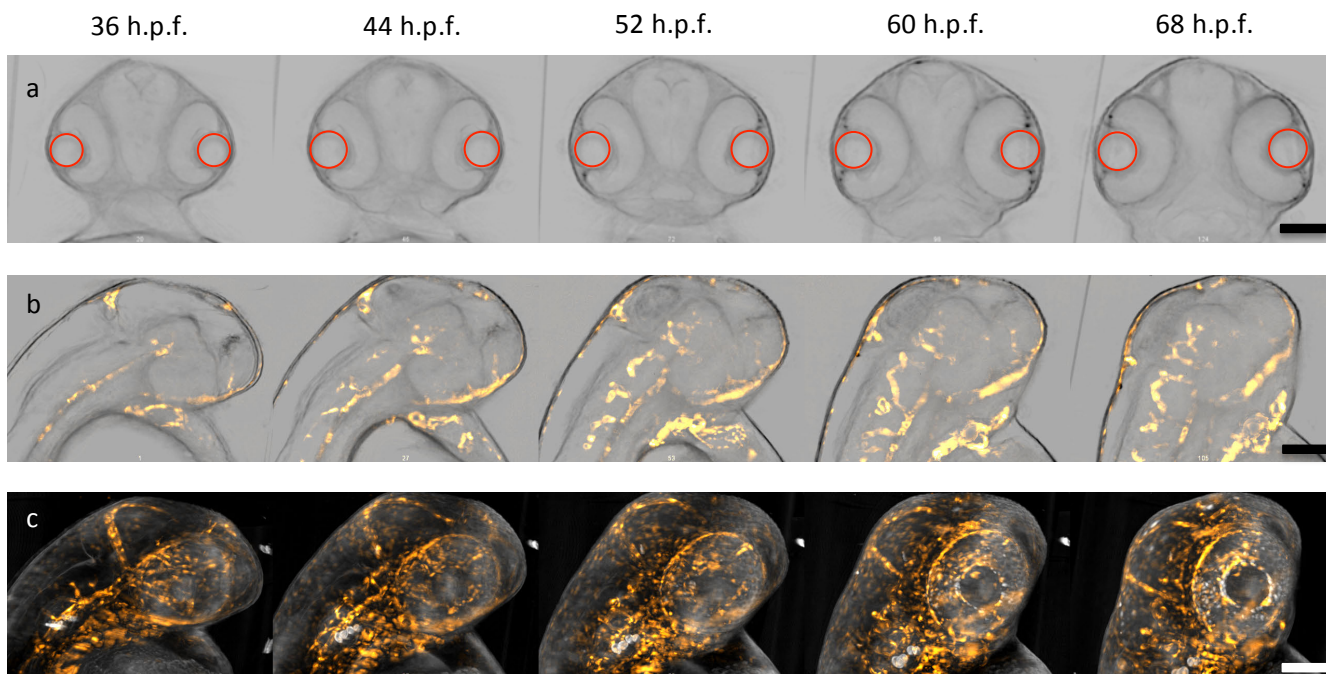


Figure S6 | Registration of time lapse acquisition

(a) Coronal sections of the sample showing the detected spheres (in red), aligned horizontally at every time point of the time lapse. **(b)** Sagittal sections of the sample obtained with optical tomography (gray) superimposed with SPIM acquisition (yellow), showing the formation of the cranial vasculature in a single plane over 1.5 days of development. **(c)** Three-dimensional reconstructions (lateral view) of fluorescence (SPIM) and bright-field contrast (tomography) during time lapse. The sample is a *Tg(fli:GFP)* zebrafish. Scale bar is 100 μm .

All images of the time-lapse reconstructions were registered to a reference system based on the fish's anatomy. The position of the eye lenses was automatically detected in the reconstructed volumes. A reference system with origin in the eyes' center of mass was defined and a rigid transformation was applied to the reconstructed volumes in order to orient the eyes of the zebrafish to the same virtual axis (horizontal) in all the time points of the time lapse (see also Movie 6). The fluorescence volumes obtained with SPIM were aligned accordingly, applying the same rigid transformation.

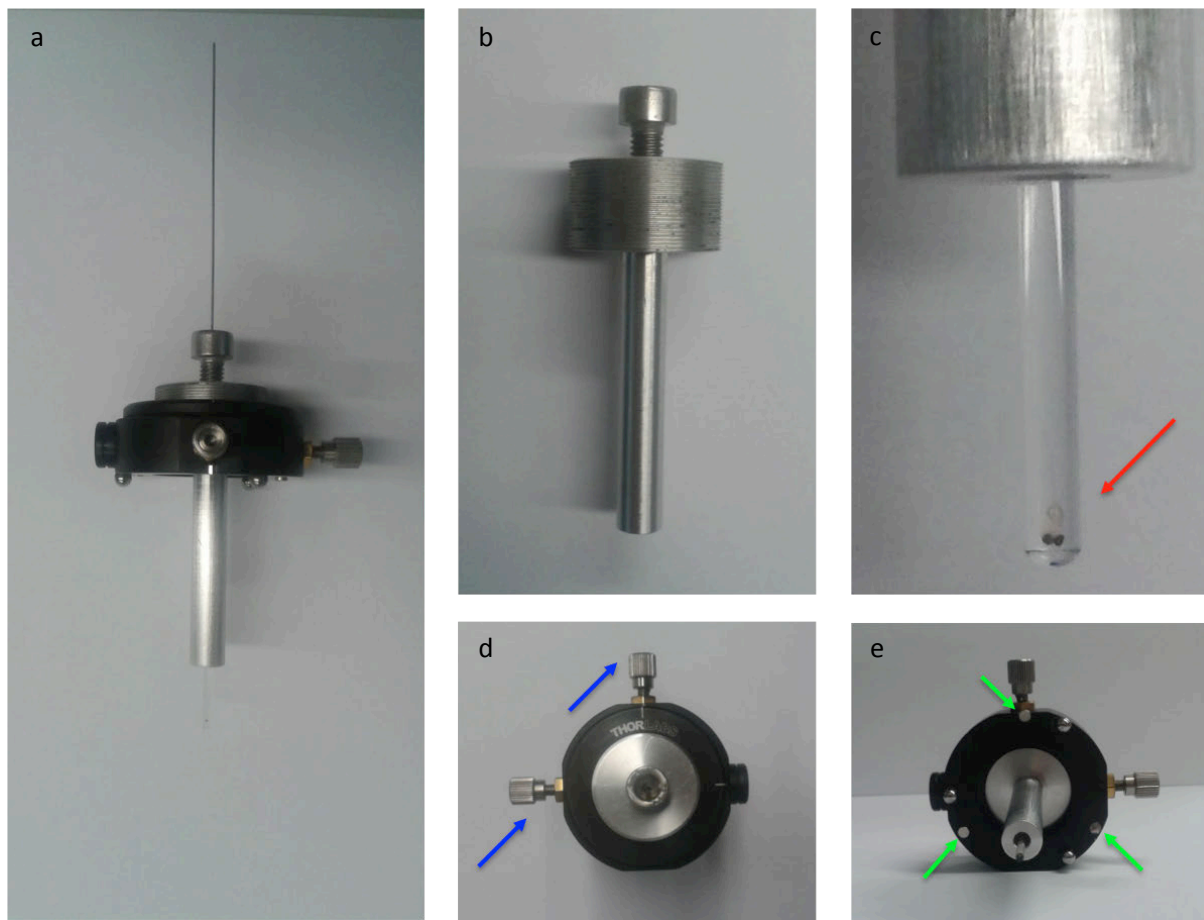


Figure S7 | Sample holder

The sample holder was constructed using a precision xy translation mount (Thorlabs, LM1XY). The two translation screws (blue arrows) were used to move the sample relative to the rotational axis of the rotating stage of the microscope (not shown) and to center the sample in the field of view during the entire 360° rotation. The translation mount was modified to incorporate three magnets to mount the sample holder on the rotating stage (green arrows). The sample (red arrow) is embedded in agarose inside a glass capillary and extruded for imaging.

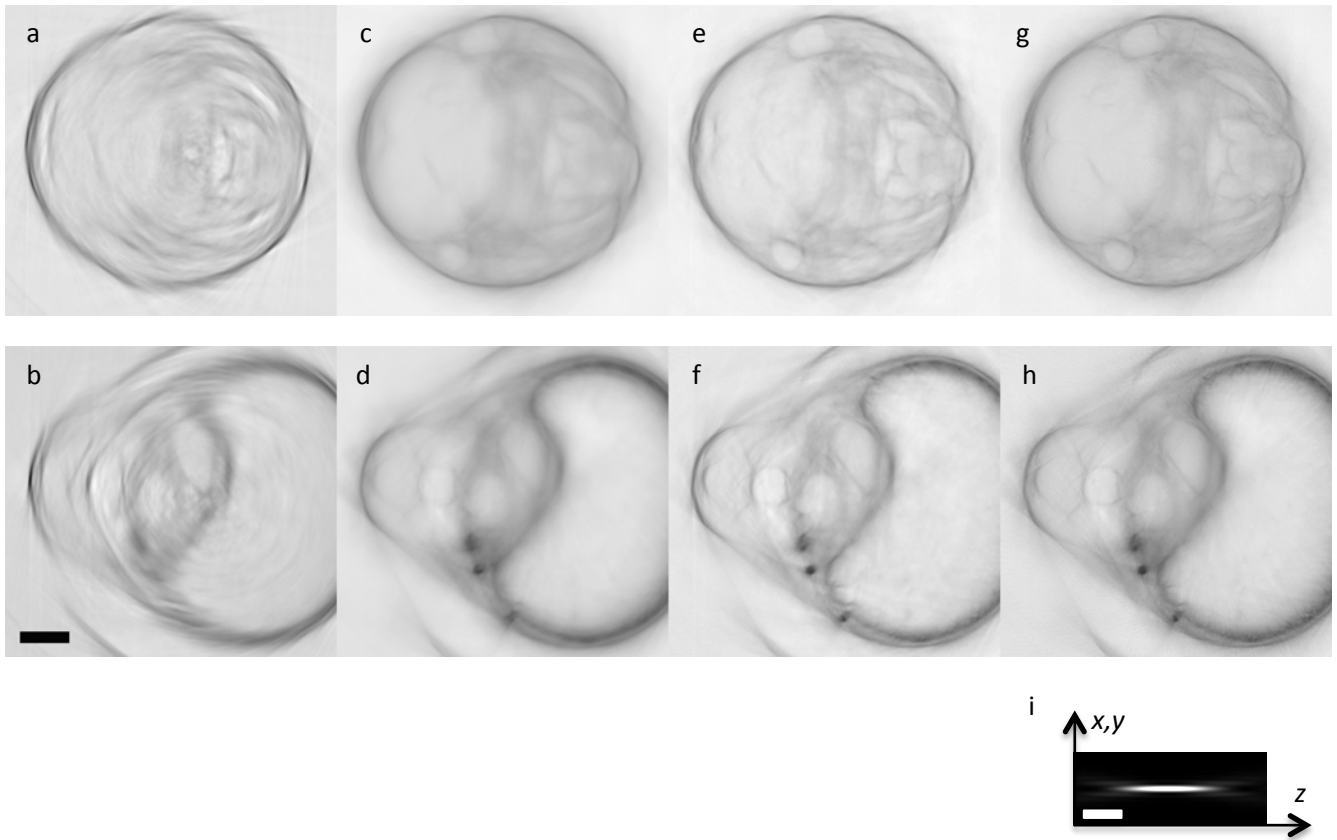


Figure S8 | Comparison of methods for depth of field extension

Reconstruction of 2 transverse sections of a 3 dpf zebrafish at two different locations in the sample: the upper panels show a single section of the head and the lower panels show a section of the trunk. At each of the 360 acquisition angles, a stack of 60 images (spaced 10 μm), was acquired and processed to create the projection. Different methods were used to generate the projections with extended depth of field. **(a,b)** No extension of the depth of field, **(c,d)** average image from full 3D stack, **(e,f)** high-pass criterion applied to the stack, **(g,h)** deconvolution applied to the stack. Scale bar is 100 μm in (a-h). **(i)** Schematic of the theoretical point spread function of the detection objective. Scale bar is 5 μm in (i).

Movie 1 | Spiral acquisition animation and raw data

During acquisition the sample is continuously translated and rotated across the image plane of the detection objective. The specimen is sampled along a spiral. The raw data acquired during the sample movement are shown on the right hand side.

Movie 2 | Tomographic reconstruction

Sagittal (left side), coronal (center) and transverse (right side) sections through a 4 dpf zebrafish (head and trunk regions) reconstructed with optical tomography. Scale bar is 100 μm .

Movie 3 | Segmented organs

Three-dimensional reconstruction of the segmented organs of a wild-type 2 dpf zebrafish head (also shown in Fig. 1 and Fig. S1). The organs are: retina (pink), eye lens (red), brain ventricles (green), brain (cyan), olfactory pit (yellow), epiphysis (blue). The raw reconstructed data are superimposed to the segmented organs, around half of the sample.

Movie 4 | Multimodal 3D reconstruction

Three dimensional reconstruction of a *Tg(neurog1:GFP)* x *Tg(kdrl:rasCherry)* at 3.5 dpf SPIM contrast (red/green) is superimposed to optical tomography (gray).

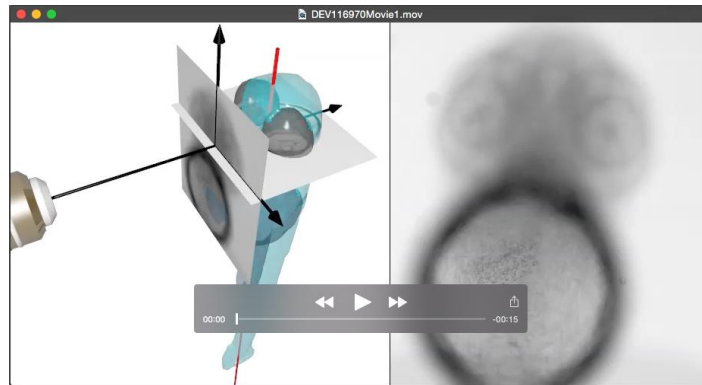
Movie 5 | Long term time lapse of development

Development of a *Tg(kdrl:GFP)* zebrafish from 16 h.p.f. to 2 dpf, observed every 10 minutes from 2 opposite views. Fluorescence is shown in yellow, brightfield contrast in gray. Scale bar is 100 μm .

Movie 6 | Registration of time lapse acquisition

Unregistered (left) and registered (right) tomographic reconstructions of a zebrafish during 1.5 days of development (maximum intensity projections). The time-lapse reconstructions were registered to a reference system based on the fish anatomy. The position of the eye lenses (shown in red) was automatically detected in all the reconstructed volumes. A reference system with the origin in the eyes' center of mass was defined (red lines) and a rigid transformation was applied to the reconstructed volumes in order to orient the eyes of the zebrafish over the same virtual axis (horizontal axis).

Movie 1



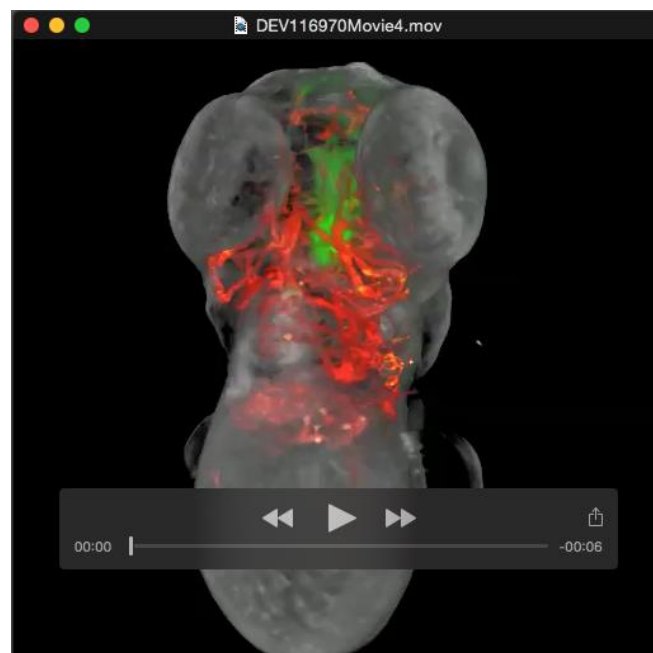
Movie 2



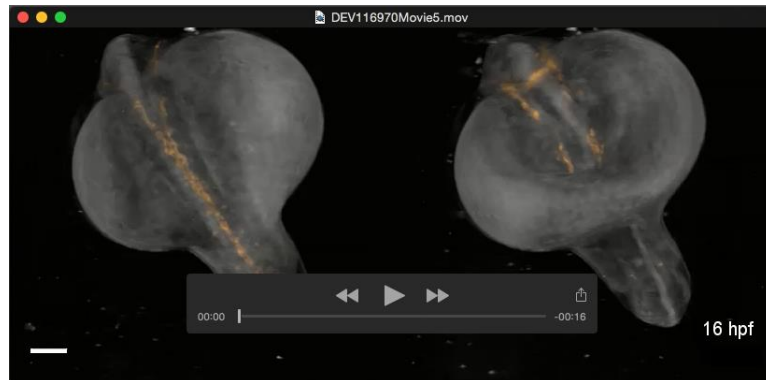
Movie 3



Movie 4



Movie 5



Movie 6

